dark parts of the two-toned rocks, the height of the largest of the bright (light-toned) rocks, and the perched rocks would suggest local deflation of 5 to 60 cm. Thus, there must have been previous deposition on this order.

References and Notes

1. Reviewed by R. Greeley, N. Lancaster, S. Lee, P. Thomas, in *Mars*, H. H. Kieffer, B. Jakosky, Eds. (Univ. of Arizona Press, Tucson, AZ, 1992), pp. 730–766.
2. S. W. Squyres *et al*., *Science* **305**, 794 (2004).
3. J. A. Crisp *et al*., *J. Geophys. Res.* **108**, 10.1029/2002JE002038 (2003).
4. M. P. Golombek *et al*., *J. Geophys. Res.* **108**, 10.1029/2003JE002074 (2003).
5. M. P. Golombek *et al*., *Lunar Planet. Sci.* **XXXV**, abstr. 2185 (2004).
6. At 0.19 (*36*), the landing site has the lowest albedo as determined from orbit of the entire landing ellipse. From analysis of broadband (0.4 to 1.0 μm) images from the MER Pancam; the average albedo measured from the surface is 0.25 ± 0.05 (*10*).
7. A martian solar day has a mean period of 24 hours 39 min 35.244 s and is referred to as a sol to distinguish this from a roughly 3% shorter solar day on Earth. A martian sidereal day, as measured with respect to the fixed stars, is 24 hours 37 min 22.663 s, as compared with 23 hours 56 min 04.0905 s for Earth. See www.giss.nasa.gov/tools/mars24/ for more information.
8. "Dust" is an imprecise term but is commonly used for material on Earth that is smaller than about 40 μm and that is transported primarily in suspension. Estimates for dust on Mars suggest diameters of a few micrometers, although these particles are thought to stick together in some cases, possibly by electrostatic charges, to form aggregates of larger sizes (*37*).
9. R. E. Arvidson *et al*., *Science* **305**, 821 (2004).
10. Names have been assigned to areographic features by the Mars Exploration Rover (MER) team for planning and operations purposes. The names are not formally recognized by the International Astronomical Union.
11. J. F. Bell III *et al*., *Science* **305**, 800 (2004).
12. K. E. Herkenhoff *et al*., *J. Geophys. Res.* **108**, 10.1029/2003JE002076 (2003).
13. J. B. Pollack *et al*., *J. Geophys. Res.* **82**, 4479 (1977).
14. P. H. Smith *et al*., *Science* **278**, 1758 (1997).
15. M. G. Tomasko, L. R. Doose, M. Lemmon, P. H. Smith, E. Wegryn, *J. Geophys. Res.* **104**, 8987 (1999).
16. P. R. Christensen *et al*., *Science* **305**, 837 (2004).
17. H. Y. McSween *et al*., *Science* **305**, 842 (2004).
18. K. E. Herkenhoff *et al*., *Science* **305**, 824 (2004).
19. J. F. Bell *et al*., *Icarus* **158**, 56 (2002).
20. J. L. Bandfield, *J. Geophys. Res.* **107**, 10.1029/2001JE001510 (2002).
21. R. P. Sharp, *J. Geol.* **71**, 617 (1963).
22. Ripples are bedforms composed of sand and granules that are moved by surface creep induced by the impact of saltating sands, whereas dunes are larger bedforms typically composed of finer sands and not formed directly by saltation processes.
23. R. Greeley *et al*., *J. Geophys. Res.* **104**, 8573 (1999).
24. M. P. Golombek, N. T. Bridges, *J. Geophys. Res.* **105**, 1841 (2000).
25. J. A. Grant *et al*., *Science* **305**, 807 (2004).
26. R. Greeley, J. D. Iversen, *Wind as a Geological Process: Earth, Mars, Venus, and Titan* (Cambridge Univ. Press, Cambridge, 1985).
27. R. Greeley, J. D. Iversen, *Geophys. Res. Lett.* **14**, 925 (1987).
28. M. R. Raupach, *Boundary-Layer Meterol.* **60**, 375 (1992).
29. M. R. Raupach, D. A. Gillette, J. F. Leyes, *J. Geophys. Res.* **98**, 3023 (1993).
30. N. T. Bridges *et al*., *J. Geophys. Res.* **104**, 8595 (1999).
31. R. Greeley *et al*., *J. Geophys. Res.* **87**, 10009 (1992).
32. N. T. Bridges *et al*., *Planet. Space Sci.* **52**, 199 (2004).
33. S. P. Gorevan *et al*., *J. Geophys. Res.* **108**, 10.1029/2003JE002061 (2003).
34. S. R. C. Rafkin, T. I. Michaels, *J. Geophys. Res.* **108**, 10.1029/2002JE002027 (2003).
35. D. Toigo, M. I. Richardson, *J. Geophys. Res.* **108**, 10.1029/2003JE002064 (2003).
36. R. Greeley *et al*., *J. Geophys. Res.* **108**, 10.1029/2002JE002006 (2003).
37. M. T. Mellon, B. M. Jakosky, H. H. Kieffer, P. R. Christensen, *Icarus* **148**, 437 (2000).
38. R. Greeley, *J. Geophys. Res.* **84**, 6248 (1979).

39. Our work was supported by NASA by contracts through the Jet Propulsion Laboratory.

10 May 2004; accepted 23 June 2004

REPORT

Localization and Physical Properties Experiments Conducted by Spirit at Gusev Crater

R. E. Arvidson,[1] R. C. Anderson,[2] P. Bartlett,[3] J. F. Bell III,[4] D. Blaney,[2] P. R. Christensen,[5] P. Chu,[3] L. Crumpler,[6] K. Davis,[3] B. L. Ehlmann,[1] R. Fergason,[5] M. P. Golombek,[2] S. Gorevan,[3] J. A. Grant,[7] R. Greeley,[5] E. A. Guinness,[1] A. F. C. Haldemann,[2] K. Herkenhoff,[8] J. Johnson,[8] G. Landis,[9] R. Li,[10] R. Lindemann,[2] H. McSween,[11] D. W. Ming,[12] T. Myrick,[3] L. Richter,[13] F. P. Seelos IV,[1] S. W. Squyres,[4] R. J. Sullivan,[4] A. Wang,[1] J. Wilson[3]

The precise location and relative elevation of Spirit during its traverses from the Columbia Memorial station to Bonneville crater were determined with bundle-adjusted retrievals from rover wheel turns, suspension and tilt angles, and overlapping images. Physical properties experiments show a decrease of 0.2% per Mars solar day in solar cell output resulting from deposition of airborne dust, cohesive soil-like deposits in plains and hollows, bright and dark rock coatings, and relatively weak volcanic rocks of basaltic composition. Volcanic, impact, aeolian, and water-related processes produced the encountered landforms and materials.

During the first few Mars solar days (sols) (*1*) of operations, we determined the landed location in inertial coordinates by analyzing Spirit-to-Earth two-way X-band Doppler transmissions and two passes of ultrahigh-frequency two-way Doppler between Spirit and the Mars Odyssey orbiter. The equivalent location in the International Astronomical Union (IAU) 2000 body-centered reference frame is 14.571892°S, 175.47848°E. The location with respect to surface features was derived by the correlation of hills and craters observed in images taken by the Pancam, the Entry Descent and Landing (EDL) Camera, and the Mars Orbital Camera. On the basis of these analyses, the landing site is located at 14.5692°S, 175.4729°E in IAU 2000 coordinates, ~300 m north-northwest of the radiometric solution. This offset is consistent with the map tie errors between inertially derived coordinate systems and those derived from image-based coverage of the planet.

Localization experiments during traverses focused on systematic acquisition of forward- and backward-looking overlapping images, onboard inertial measurement unit (IMU) observations to derive rover tilt, and tracking the number of wheel turns to provide wheel-based odometry. These observations were employed in a least-squares bundle adjustment to solve for the position and orientation of Spirit in local Cartesian coordinates at discrete locations during traverses (Fig. 1 and Plate 14). In addition, measurements of differential rocker and bogie angles in the suspension system, together with IMU data, were used to reconstruct the elevation of each wheel at a 2- to 8-Hz sample rate relative to the start of each traverse (Fig. 1).

Localization results were extracted for 33 traverse segments from the Columbia Memori-

[1]Department of Earth and Planetary Sciences, Washington University, St. Louis, MO 63130, USA. [2]Jet Propulsion Laboratory, California Institute of Technology, Pasadena, CA 91109, USA. [3]Honeybee Robotics, 204 Elizabeth Street, New York, NY 10012, USA. [4]Department of Astronomy, Space Sciences Building, Cornell University, Ithaca, NY 14853, USA. [5]Department of Geological Sciences, Arizona State University, Tempe, AZ 85287, USA. [6]New Mexico Museum of Natural History and Science, Albuquerque, NM 87104, USA. [7]Center for Earth and Planetary Studies, National Air and Space Museum, Smithsonian Institution, Washington, DC 20560, USA. [8]U.S. Geological Survey, Flagstaff, AZ 86001, USA. [9]National Aeronautics and Space Administration (NASA) Glenn Research Center, Cleveland, OH 44135, USA. [10]Department of Civil and Environmental Engineering and Geodetic Science, Ohio State University, Columbus, OH 43210, USA. [11]Department of Earth and Planetary Sciences, University of Tennessee, Knoxville, TN 37996, USA. [12]NASA Johnson Space Center, Houston, TX 77058, USA. [13]Deutsche Luft und Raumfahrt Institut für Raumsimulation, Linder Hoehe, Koln, DJ-51170, Germany.

al station to the rock Route 66 (*2*) (Fig. 1). The terrain from the landing site to the location of the rock Humphrey in Middle Ground hollow is flat and level, with a relative-elevation decrease of only 1 m over the horizontal distance of 197 m between localization stations. From Humphrey to the crater rim, the relative elevation increased 7.4 m over a distance of 135 m between stations, consistent with the increased slope expected as the rim of Bonneville crater was approached. From the crater rim to the rock Mazatzal, the relative elevation decreased 0.6 m over a distance of 80 m, consistent with the traverse azimuths that kept the vehicle near the rim. Finally, the distance from Mazatzal to Route 66 is 95 m, with a decrease in relative elevation of 3 m, consistent with travel away from the rim. Based on wheel odometry, Spirit traversed 637 m from Columbia Memorial station to the rock Route 66 and the summed distance between the 33 stations is 507 m. Notably, the bundle adjustments increased positional accuracy by 2% relative to the use of wheel odometry alone.

Rocks litter the landscape at the landing site and are larger and more abundant near the Bonneville crater rim (*3*). Soil (*4*) deposits dominated by particles <1 mm in diameter cover the plains and occasionally are found as aeolian drifts (*3*, *5*, *6*). Soil deposits not within hollows or on hollow rims are covered with an evenly spaced set of angular to smooth rocks ranging in size from granules (2 to 4 mm) to pebbles (4 to 16 mm). Furthermore, soils are covered with a thin (<1-mm) layer of bright red dust. These dust deposits are easily disturbed, as shown by airbag bounce marks generated during landing and observations that wheel motions associated with traversing removed the dust covers and exposed darker, underlying deposits (Fig. 1). The short-circuit current monitor solar cell showed a decrease in current of 0.2% per sol (corrected for seasonal variations in Mars-Sun distance and solar elevation angle) over the first 93 sols of operation, showing airborne dust accumulation on the rover solar panels comparable to that observed during the Pathfinder mission (*7*). The ubiquitous nature of the dust cover on soils, combined with discernable dust accumulation rates, serves as evidence that the Gusev site has accumulated dust deposits for a number of years.

Soil deposits typically display surface crusts a few millimeters thick beneath the thin dust covers. For example, airbag retraction scars include thin crustal plates a few centimeters in width that were laterally displaced as the deflated airbags were retracted after landing. Surface crusts also have been observed in wheel track disturbances, especially where rocks wobbled by wheels created moats as small amounts of adjacent crust were displaced. Imaging of wheel tracks shows well-defined soil casts indicative of materials with a range of grain sizes, from coarse sand (0.5 to 1 mm) to diameters too fine to be discerned with the 30 μm/pixel spatial resolution of the Microscopic Imager (MI) (Fig. 2A). Imaging data also show that smooth indentations were produced by the Mössbauer Spectrometer contact plate as it pushed into soils before the contact switch initiated, stopping movement at ~1 N of applied force (Fig. 2A). The finer grains were molded into interstices of the larger grains when displaced by the wheels and faceplate, producing well-defined soil casts. Unfortunately, no in situ measurements have been done yet on cloddy soils that are dust free. Thus, it is impossible to determine whether the cloddy nature is due to enrichment of cementing agents such as iron oxides or sulfates.

To explore the degree to which soil properties change with depth, a 6- to 7-cm-deep trench was excavated with the right front wheel in Laguna hollow on sol 47. Trench walls in Laguna hollow have slopes of up to 65°, values steeper than the angle of repose for most granular materials (~30°). This result indicates the presence of slightly cohesive soils throughout the upper 6 to 7 cm beneath the surface, although the exact degree of cohesion is difficult to estimate with certainty. An additional experiment excavated into the drift Serpent (Fig. 2B). The surface layer of the drift consists of closely packed, very coarse sand-sized particles (~1 to 2 mm in diameter) overlying finer grained soils. The very coarse sand armors the surface and protects the drift from aeolian erosion and transport of the underlying particles. The armor is covered with the thin dust deposit that is typical of the soil surfaces examined during Spirit's traverses and observations. The slightly cohesive nature of the upper portion of the drift soil is evident based on the presence of clods produced by the excavations (Fig. 2).

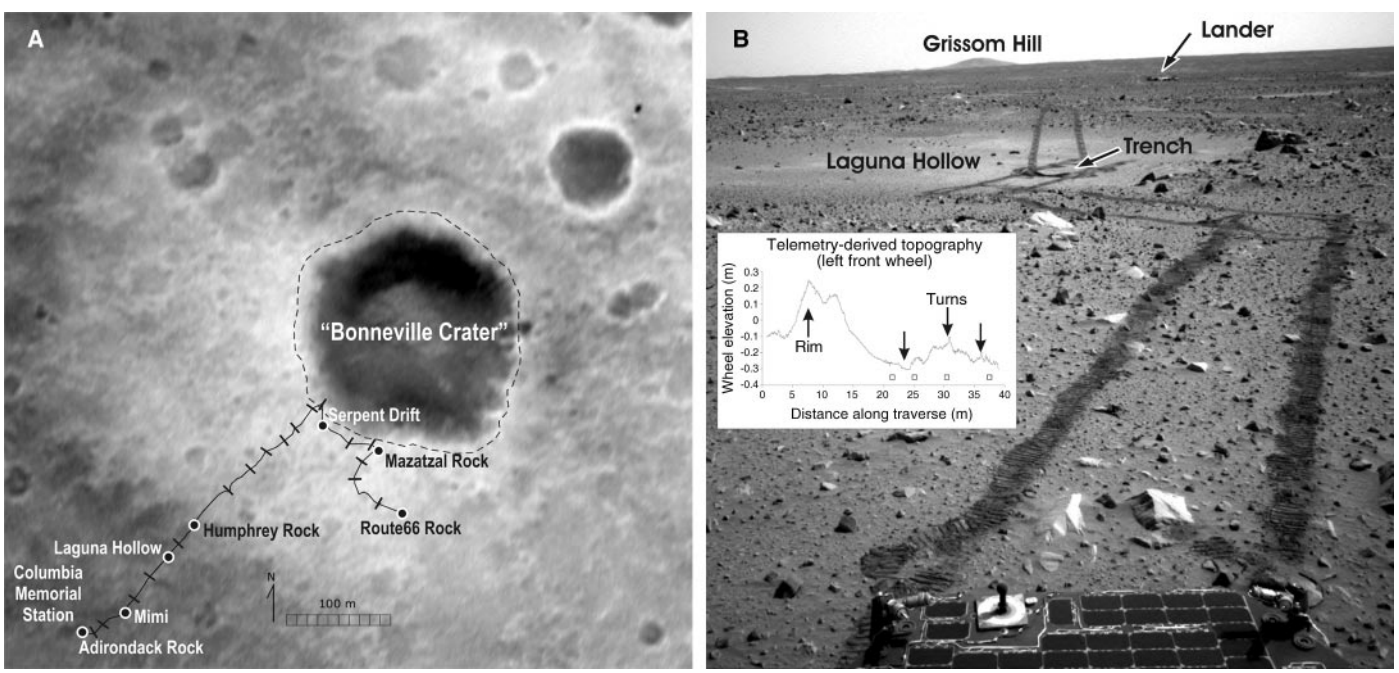

Fig. 1. (**A**) MER EDL Camera image acquired from 1430 m above the surface shows Spirit's localization-derived traverses and positions for physical property experiments during the first 93 sols in Gusev crater. Tick marks along traverse path show localization stations. Some stations that are close together are not plotted to avoid clutter. Image identification is 2E126462405EDN0000F0006N0M1. (**B**) Navcam image (2N130812149EFF1000P1901L0M1) of Laguna hollow with tracks that are about 10 cm wide. The inset shows a vertical topographic profile across the hollow as derived from rover tilt and wheel suspension data.

With regard to standard terramechanical analyses, estimates of soil-bearing strength of ~5 kPa, cohesive strength of ~1 kPa, and an angle of internal friction of ~20° were derived from wheel sinkage depths in a hollow adjacent to the lander traversed on sol 15 (*8*). More resistant deposits (with less sinkage), such as those found in the egress area traversed on sol 12 and in the region in front of the drift Arena crossed on sol 42, provided values of ~200 kPa, 15 kPa, and 25°, respectively, for the same parameters. These values are comparable to the range of soil values found from analyses of Viking Lander and Pathfinder physical properties data (*9*).

Rocks ranging up to boulder sizes were observed during Spirit's traverses (Fig. 1). Rocks tend to be massive in appearance, although a few rocks, including Mimi (Fig. 2A), have a layered appearance. The layered rocks are interpreted to be weathered in place by mechanical spalling along lines of weakness. Low-lying rocks (less than ~25 cm tall) of the more typical massive variety in many cases appear to have been faceted by wind action and tend to be light-toned relative to surrounding soils, e.g., Mazatzal rock on the rim of Bonneville crater (Fig. 3). Additionally, these rocks are commonly embedded in soil deposits. All rocks show strong variations in brightness with lighting and viewing geometries in imaging data. At small phase angles, flat surfaces of individual rocks tend to be brighter and redder in visible wavelengths relative to corners or edges or tops, consistent with the presence of brighter coatings that are optically thicker on the facets as opposed to the corners or edges. These observations imply that rocks are coated with bright, red materials preferentially on smooth, flat facets. Accumulation of airborne dust is a plausible mechanism for formation of these bright coatings.

Rock Abrasion Tool (RAT) deployments were made on Adirondack (~20-cm-high light-toned rock), Humphrey (~50-cm-high rock, variable brightness), and Mazatzal (~20-cm-high, faceted, light-toned rock) (Figs. 1 and 3). After initial brushing experiments designed to remove loose deposits, the RAT was used to grind into the rock facets, extending 2.7 and 2.1 mm (based on RAT motor drive data) into Adirondack and Humphrey, respectively. For Mazatzal, two rattings were conducted with a

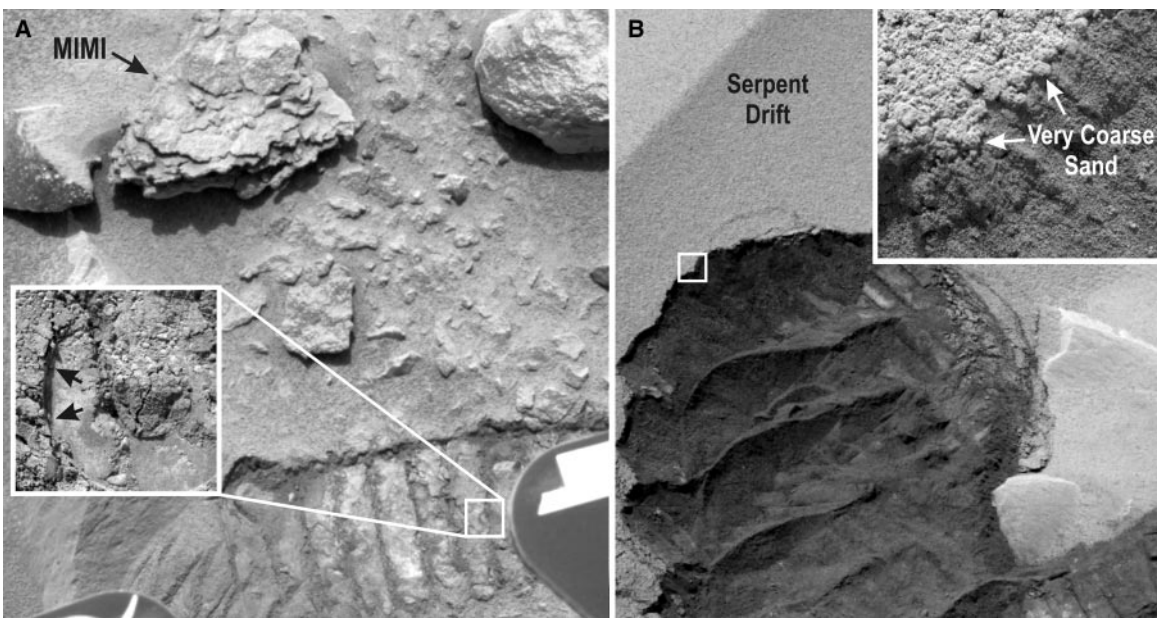

Fig. 2. (**A**) Pancam image (2P130088011-EFF0514P2538L2M1) of Mimi rock and rover front wheel tracks, along with an MI (2M-130169106EFF0514-P2953M2M1) inset showing the tracks in more detail. The MI inset shows the imprint of the MB contact plate (arrows) into moldable soil. The inset covers about 3 cm across. (**B**) Pancam image (2P13-2756681EFF1957P23-52L2M1) of Serpent drift after scuffing by the rover front wheel, with MI (2M132842-058EFF2000P2977M-2M1) inset showing dust-coated armor of very coarse sand grains over sand-sized and finer-grained particles. Soil clods are evident just to the upper right of the inset location. The MI inset covers about 1.5 cm in width on the drift.

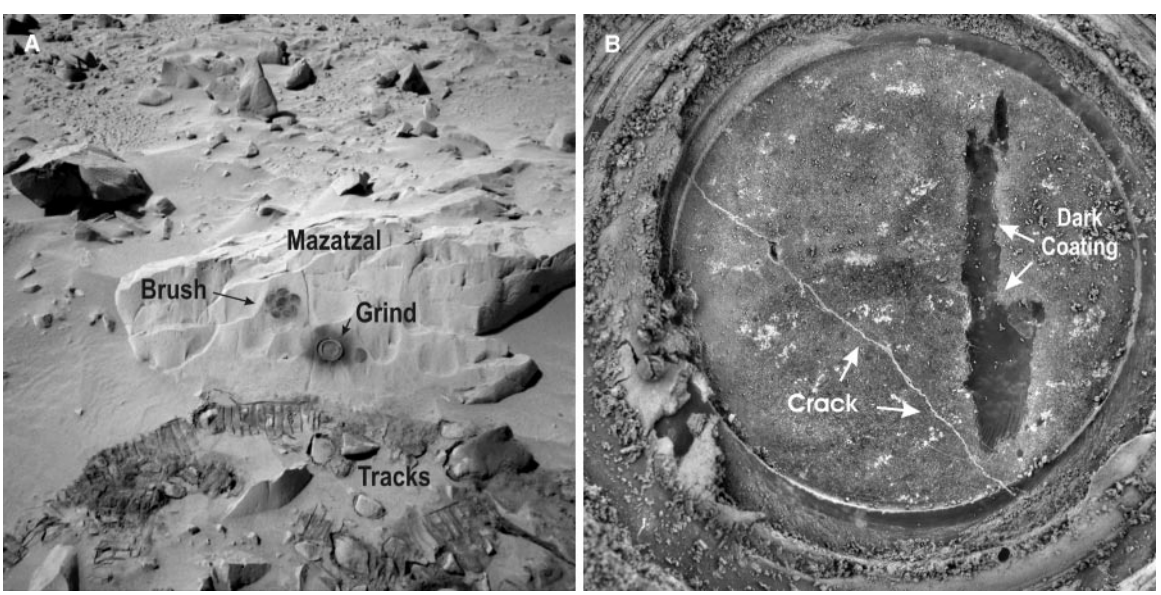

Fig. 3. (**A**) Navcam image (2N13400813-9EFF2238P1959L0M1) showing the brushed (Brush) and abraded (Grind) areas on the 2.3-m-wide Mazatzal rock. (**B**) Mosaic (2M-P085IOF22ORT32P2-959L456F1_qn) of four MI images acquired of the Mazatzal RAT hole after the second grinding operation, showing that only a small amount of dark coating remains. The RAT hole is about 4.5 cm across. Black and white version of merged color Pancam and MI mosaic is shown.

3.8-mm penetration on the first attempt and a 4.1-mm penetration on the second attempt. The brushing and grinding operations on Mazatzal showed the presence of a dark, smooth, indurated coating beneath the light-toned loose coating (Fig. 3). This dark coating was largely removed by the second grinding, revealing the underlying rock surface (Fig. 3B). There is also some evidence that a second bright coating may underlie the dark coating (*10*, *11*).

Grind motor currents, the depths achieved, and grinding areas provided estimates of the amount of energy consumed by the RAT while removing a unit volume of material. Because grind energy density is a nontraditional means of quantifying rock mechanical properties, three terrestrial rocks were abraded in the laboratory for calibration, with the use of a flight-like RAT: a fresh, nonvesicular basalt sample from Ash Fork, Arizona; a fine-grained dolostone sample collected from the Soda Mountains north of Silver Lake, California; and Cleveland Member (fissle shale) of the Ohio Formation. These experiments yielded energy densities of ~166, 83, and 11 J/mm^3, respectively. For comparison, Humphrey required 83 J/mm^3, whereas Adirondack and Mazatzal required 51 and 65 J/mm^3, respectively. Thus, rocks abraded by Spirit required less energy per volume than the particular basalt sample ground in the tests, and comparable grind energy densities to the two terrestrial sedimentary rock samples, even though composition and mineralogy data from Spirit demonstrate that the rocks encountered are basalts (*10*, *12*–*14*).

The physical properties experiments conducted by Spirit at Gusev crater show that surface soils are cloddy, rock coatings are ubiquitous, and rocks are easily abraded and thus mechanically weaker than the fresh, nonvesicular basaltic sample used in the laboratory tests. Furthermore, the abraded surfaces of the rocks at Gusev exposed vugs and cracks filled with bright material suggestive of aqueous mineralization (Fig. 3) (*10*, *11*). There is also a suggestion of a vertical weathering profile for Humphrey rock, where the grinding direction was accomplished at a slight angle from the surface normal, thereby exposing shallow to deep surfaces (*10*). The presence of liquid water, even for brief periods of time, is one way to cement surface soils, form rock coatings, deposit minerals in vugs and cracks, and weather the surfaces of rocks. Liquid water might occur for brief periods when the spin axis obliquity and atmospheric relative humidity are high and precipitation occurs as snow or frost (*15*). A modest temperature enhancement as a result of absorption of solar radiation by underlying regolith and rocks, with "greenhouse"-related absorption of outgoing thermal radiation by the ice and snow, could generate thin films of liquid water that would mobilize soluble species and produce the features observed by Spirit. Other models are also being explored to place the physical properties experiments in an environmental context, in addition to further measurements designed to test hypotheses.

References and Notes

1. A martian solar day has a mean period of 24 hours 39 min 35.244 s and is referred to as a sol to distinguish this from a roughly 3% shorter solar day on Earth. A martian sidereal day, as measured with respect to the fixed stars, is 24 hours 37 min 22.663 s, as compared with 23 hours 56 min 04.0905 s for Earth. See www.giss.nasa.gov/tools/mars24 for more information.
2. Names have been assigned to areographic features by the Mars Exploration Rover (MER) team for planning and operations purposes. The names are not formally recognized by the IAU.
3. J. A. Grant *et al.*, *Science* **305**, 807 (2004).
4. The term martian soil is used here to denote any loose unconsolidated materials that can be distinguished from rocks, bedrock, or strongly cohesive sediments. No implication of the presence or absence of organic materials or living matter is intended.
5. P. R. Christensen *et al.*, *Science* **305**, 837 (2004).
6. R. Greeley *et al.*, *Science* **305**, 810 (2004).
7. G. Landis, P. Jenkins, *J. Geophys. Res.* **105**, 1855 (2000).
8. Based on wheel track sinkage values for terrains covered by one to three MER wheels described in L. Richter and P. Hamacher, paper presented at the 13th Conference of the International Society for Terrain-Vehicle Systems, Munich, Germany, 14 to 17 September 1999.
9. H. Moore *et al.*, *J. Geophys. Res.* **104**, 8729 (1999).
10. K. E. Herkenhoff *et al.*, *Science* **305**, 824 (2004).
11. H. Y. McSween *et al.*, *Science* **305**, 842 (2004).
12. S. W. Squyres *et al.*, *Science* **305**, 794 (2004).
13. J. F. Bell III *et al.*, *Science* **305**, 800 (2004).
14. P. R. Christensen *et al.*, *Science* **305**, 837 (2004).
15. M. A. Mischna *et al.*, *J. Geophys. Res.* **108**, 5062 (2003).
16. Work funded by NASA through the Mars Exploration Rover Project. We thank the MER team of scientists and engineers, who made the landing, traverses, and science observations a reality.

4 May 2004; accepted 2 July 2004

REPORT

Textures of the Soils and Rocks at Gusev Crater from Spirit's Microscopic Imager

K. E. Herkenhoff,[1]* S. W. Squyres,[2] R. Arvidson,[3] D. S. Bass,[4] J. F. Bell III,[2] P. Bertelsen,[5] N. A. Cabrol,[6] L. Gaddis,[1] A. G. Hayes,[2] S. F. Hviid,[7] J. R. Johnson,[1] K. M. Kinch,[8] M. B. Madsen,[5] J. N. Maki,[4] S. M. McLennan,[9] H. Y. McSween,[10] J. W. Rice Jr.,[11] M. Sims,[12] P. H. Smith,[13] L. A. Soderblom,[1] N. Spanovich,[13] R. Sullivan,[2] A. Wang[14]

The Microscopic Imager on the Spirit rover analyzed the textures of the soil and rocks at Gusev crater on Mars at a resolution of 100 micrometers. Weakly bound agglomerates of dust are present in the soil near the Columbia Memorial Station. Some of the brushed or abraded rock surfaces show igneous textures and evidence for alteration rinds, coatings, and veins consistent with secondary mineralization. The rock textures are consistent with a volcanic origin and subsequent alteration and/or weathering by impact events, wind, and possibly water.

The Microscopic Imager (MI) is a fixed-focus camera mounted on a robotic arm (*1*, *2*). The MI was designed to function like a geologist's hand lens, acquiring images at a spatial resolution of 31 μm/pixel (picture element) over a broad spectral range (400 to 700 nm). The MI uses the same electronics design as the other Mars Exploration Rover (MER) cameras (*3*, *4*), but its optics yield a field of view of 32 by 32 mm across a 1024- by 1024-pixel charge-coupled device image. The MI acquires images with only solar or skylight illumination of the target surface. A contact sensor is used to place the MI slightly closer to the target surface than its best-focus distance of about 66 mm, which allows concave surfaces to be imaged in good focus. The depth of field of the MI is ~3 mm; coarse focusing (~2-mm precision) is achieved by moving the arm away from a rock target after contact is sensed. The MI optics are protected from the martian environment by a retractable dust cover. This cover includes a Kapton (polyimide film, DuPont, Wilmington, Delaware) window that is tinted orange to restrict the spectral bandpass to 500 to 700 nm, which allows crude color information to be obtained by acquiring images with the cover open and closed.